jmb Article

Effect of Mimetic CDK9 Inhibitors on HIV-1-Activated Transcription

Rachel Van Duyne[1,2], Irene Guendel[1], Elizabeth Jaworski[1], Gavin Sampey[1], Zachary Klase[3], Hao Chen[4], Chen Zeng[4,5], Dmytro Kovalskyy[6], Mahmoud H. el Kouni[7], Benjamin Lepene[8], Alexis Patanarut[8], Sergei Nekhai[9], David H. Price[10] and Fatah Kashanchi[1]

1 - National Center for Biodefense and Infectious Diseases, *George Mason University, Manassas, VA 20110, USA*
2 - Department of Microbiology, *Immunology, and Tropical Medicine, The George Washington University Medical Center, Washington, DC 20037, USA*
3 - Molecular Virology Section, *Laboratory of Molecular Microbiology, NIAID, National Institutes of Health, Bethesda, MD 20892-0460, USA*
4 - Department of Physics, *The George Washington University, Washington, DC 20052, USA*
5 - Department of Physics, *Huazhong University of Science and Technology, Wuhan 430074, China*
6 - Protein Engineering Department, *Institute of Molecular Biology and Genetics, UAS, Kiev, Ukraine*
7 - Department of Pharmacology and Toxicology, *Center for Aids Research, Comprehensive Cancer Center, University of Alabama at Birmingham, Birmingham, AL 35294, USA*
8 - Ceres Nanosciences, *Inc., Manassas, VA 20110, USA*
9 - Department of Medicine, *Center for Sickle Cell Disease, Howard University, Washington, DC 20060, USA*
10 - Department of Biochemistry, *Interdisciplinary Molecular Biology Program, University of Iowa, Iowa City, IA, USA*

Correspondence to Fatah Kashanchi: *National Center for Biodefense and Infectious Diseases, George Mason University, Discovery Hall, Room 182, 10900 University Boulevard MS 1H8, Manassas, VA 20110, USA. fkashanc@gmu.edu*
http://dx.doi.org/10.1016/j.jmb.2012.12.005
Edited by E. O. Freed

Abstract

Potent anti-retroviral therapy has transformed HIV-1 infection into a chronic manageable disease; however, drug resistance remains a common problem that limits the effectiveness and clinical benefits of this type of treatment. The discovery of viral reservoirs in the body, in which HIV-1 may persist, has helped to explain why therapeutic eradication of HIV-1 has proved so difficult. In the current study, we utilized a combination of structure-based analysis of cyclin/CDK complexes with our previously published Tat peptide derivatives. We modeled the Tat peptide inhibitors with CDKs and found a particular pocket that showed the most stable binding site (Cavity 1) using *in silico* analysis. Furthermore, we were able to find peptide mimetics that bound to similar regions using *in silico* searches of a chemical library, followed by cell-based biological assays. Using these methods, we obtained the first-generation mimetic drugs and tested these compounds on HIV-1 long terminal repeat-activated transcription. Using biological assays followed by similar *in silico* analysis to find second-generation drugs resembling the original mimetic, we found the new targets of Cavity 1 and Cavity 2 regions on CDK9. We examined the second-generation mimetic against various viral isolates and observed a generalized suppression of most HIV-1 isolates. Finally, the drug inhibited viral replication in humanized mouse models of $Rag2^{-/-}\gamma c^{-/-}$ with no toxicity to the animals at tested concentrations. Our results suggest that it may be possible to model peptide inhibitors into available crystal structures and further find drug mimetics using *in silico* analysis.

Introduction

Current anti-retroviral therapies consist of a cocktail of drugs designed to prevent HIV-1-infected cells from producing actively replicating virus. This highly active anti-retroviral therapy considerably decreases HIV-1-related diseases, morbidity, and mortality as well as significantly improves the quality of life of responsive patients. This treatment, though effective, is not robust enough to eliminate HIV-1

from infected individuals; indeed, if an HIV-1-infected individual ceases highly active anti-retroviral therapy treatment, viremia dramatically increases over a short period of time. The existence of a latent reservoir of HIV-1-infected cells is one of the major hurdles in designing appropriate and effective therapies to rid an HIV-1-infected individual of all viruses. Novel model systems of HIV-1 latency need to be developed, both *in vivo* and *in vitro*, in order to effectively develop such therapies.

The chronic phase of infection is also marked by the presence of latently infected cells that contain an integrated HIV-1 provirus and are transcriptionally silent but can be activated to generate infectious virus and support a productive infection. Activation of HIV-1 long terminal repeat (LTR) transcriptional elongation occurs following the recruitment of Tat to the transcription machinery via a specific interaction with TAR (*trans*-acting-responsive RNA element), a 59-residue RNA leader sequence that folds into a specific stem–loop structure. After binding to TAR RNA, Tat stimulates a specific protein kinase called TAK (Tat-associated kinase). The kinase subunit of TAK, CDK9, is analogous to a component of a positive-acting elongation factor isolated from *Drosophila* called p-TEFb.[1] Human p-TEFb is a member of a multi-protein complex found in two distinct forms: a small, active p-TEFb that contains CDK9 with a cyclin partner and a large, inactive p-TEFb that also contains 7SK small nuclear RNA, the HEXIM1, MePCE, and LARP7 proteins.[2–4] Cyclin-dependent kinases contain a conserved threonine in their T-loop, and phosphorylation of this residue induces a conformational change that allows CDK substrates to access the catalytic core of the enzyme. In a recent crystal structure of the complex, it has been shown that Tat interacts predominantly not only with cyclin T1 but also with the T-loop of CDK9.[5] Thus, Tat inserts itself into the interface of CDK9 and cyclin T1 to further stabilize the CDK9/cyclin T1 complex.

Using a series of Tat peptide analogs containing various amino acid substitutions in the core domain, we previously found an inhibitory set of peptides that could effectively inhibit Tat transactivation of the HIV-1 promoter. The inhibition was specific to a short 15-mer Tat peptide and we were ultimately able to truncate the residues to a 5-mer with equal inhibitory activity. Most notably, the Tat peptide analog 41/44 exhibited an 87-fold suppression of Tat transactivation.[6] As controls, we also tested these peptides on seven other promoters including HTLV-I, CMV, PTHrP, IgH, RAS, RSV, and SIV CAT constructs and observed preferential effect only on the HIV-1 promoter. To define the mechanism of inhibition, we devised a series of *in vivo* chromatin immunoprecipitation assays followed by PCR with specific primers to HIV-1 and glyceraldehyde 3-phosphate dehydrogenase (GAPDH) as a control. We found that both 41/44 linear and cyclized Tat peptides efficiently inhibited the serine 5 phosphorylation and not the serine 2 phosphorylation of the C-terminal domain (CTD) of RNA polymerase II (Pol II). Consistent with the inhibition of serine 5, levels of HIV-1 RNA capping and elongation by the transcription elongation factor SPT-5 were reduced in the presence of the Tat 41/44 peptide. These peptides, however, did not affect the RNA Pol II, capping, or elongation of the cellular genes such as GAPDH.[6] This was consistent with our hypothesis that the peptide 41/44 inhibited phosphorylation of RNA Pol II elongation by disrupting the cyclin/CDK complex *in vivo*.

In this article, we describe the utility of a combination of structure-based analysis of CDKs along with previously published Tat peptide derivatives and find residues of the cyclin/CDK interface that could potentially be dissociated *in vitro*. We searched for synthetic small molecules (first- and second-generation drugs) that could mimic the inhibitory peptide effects both *in vitro* and *in vivo*. Using three pharmacophore models, we identified inhibitors that effectively bind to CDK9 and inhibit HIV-1 transcription both *in vitro* and *in vivo*.

Results

Tat peptide inhibitors of CDK2 and CDK9

We previously have utilized an immobilized biotin pull-down assay to identify short Tat-derived peptides that target DNA-PK, CDK9, and CDK2.[7] In particular, two double mutants, TAALS and LAALS of the wild-type Tat peptide TKALG (K41A and G44S), are potent kinase inhibitors that disrupt the cyclin/CDK complex formation. Specifically, in functional kinase inhibition assays using the CTD of RNA Pol II as a substrate, we observed an IC_{50} of 26.1 μM for TAALS and 4.26 μM for LAALS peptides.[8] Using a series of alanine mutagenesis on CDK2, we demonstrated that these peptides interact with CDK2 directly at a binding pocket near the interface of the cyclin/CDK complex,[6] a result also obtained by computational docking programs whose docking conformation is displayed in Fig. 1a, where two key residues of CDK2, Lys178 and Tyr180, required for the binding interaction are labeled.[6]

Given the close homology at the interface of cyclin/CDK interaction sites for CDK2 and CDK9[9] as shown in Fig. 1a and b, it is conceivable that these peptides also target CDK9 in a similar fashion. Indeed, this was consistent with the result obtained by computationally docking LAALS to CDK9 as shown in Fig. 1b (see Peptide docking for details). To verify experimentally the direct binding of LAALS to CDK9 without its cyclin partner, we designed an experiment where glutathione *S*-transferase (GST)-

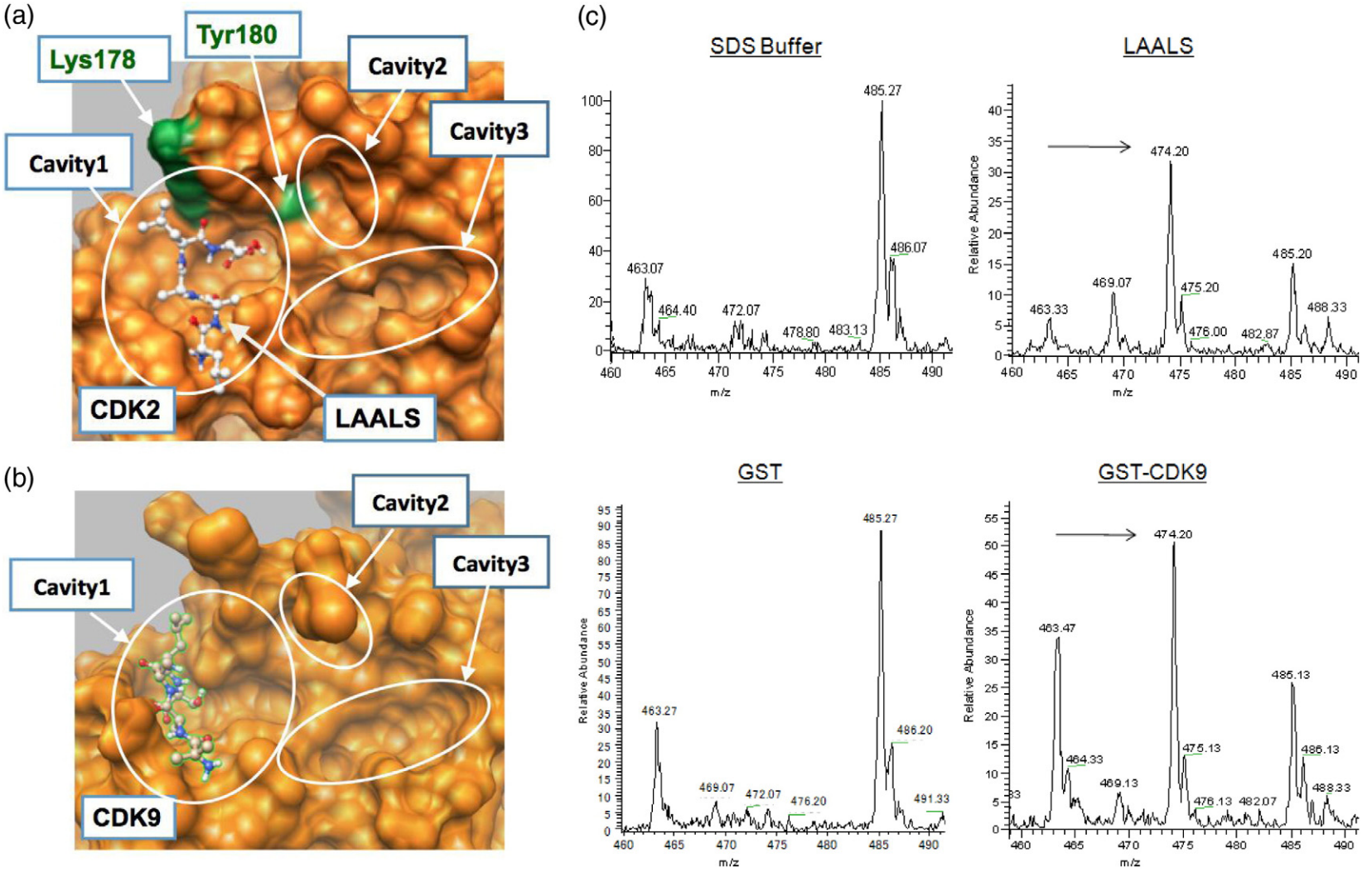

Fig. 1. Cavities at the interface binding pocket. The surfaces of CDKs are shown in orange. (a) Details of the interface binding pocket of CDK2 reveal finer structures of three distinct cavities. The peptide LAALS docks onto Cavity 1 in simulations. Two residues, Lys178 and Tyr180, are also labeled. (b) Three-cavity structure of the interface pocket on CDK9. Note that Cavity 2 is partially obscured by Leu176 on CDK9 in this perspective. Expectedly, the peptide LAALS also docks onto Cavity 1 in the simulation given the similarity of the interface pockets on CDK2 and CDK9. (c) GST-CDK9 and GST were expressed and purified twice over glutathione Sepharose beads. Peptides (50 μg) were allowed to bind various purified bead-GST proteins (2 μg) overnight at 4 °C, washed the next day, and eluted with 20 μl of elution buffer. Following centrifugation, eluates were used for further analysis using zip tip and then processed using an ESI-MS LCQ DecaXP Plus Thermo Finnigan mass spectrometer. Data are shown as *m*/*z* values zoomed in to the appropriate mass range. Arrows indicate the detection of LAALS peptide.

CDK9 (experimental) or GST alone (control) was bound to the peptide and subsequently washed with a low stringency buffer. Any bound peptides were then eluted using the same binding buffer plus 0.01% SDS. Eluted peptides from the supernatant were cleaned using zip tips (to remove salts and detergent) and then subjected to LCQ liquid chromatography/mass spectrometry (Thermo, Hercules, CA) for detection. Results of such an experiment are shown in Fig. 1c, where the buffer alone had a set of certain background molecular weight peaks (nonspecific peaks, i.e., 463.07, 485.27, and 486.07), and a similar set of peaks was also observed (with varying intensity) in the GST pull-down experiment. However, the specific LAALS peptide appeared only in the GST-CDK9 but not in the GST eluates. The LAALS peptide molecular weight is 474.20. Other control experiments, including the use of wild-type peptides or a retinoblastoma peptide that normally is not phosphorylated by CDK9, showed no binding using this assay (data not shown).

Discovery of small-molecule inhibitor F07 disrupting the cyclin/CDK interface

The above studies demonstrated that the peptide inhibitors targeted the interface pocket of the cyclin/CDK complex. This interface could then potentially serve as targets to develop small-molecule inhibitors. To search for such inhibitors by virtual screening, we analyzed the structures of CDK2 complex with cyclin E [Protein Data Bank (PDB) ID: 1W98] and with cyclin A (PDB ID: 2UUE) in order to define putative binding sites for small molecules. The overall binding area at the interface is fairly flat with three shallow cavities as already shown in Fig. 1a. The cavity formed by Ala116, His119, Ser120, Thr182, Ile186, and Ser276–Lys278 residues (i.e., Cavity 3, as shown in Fig. 2a, which centers on the hydroxyl oxygen of Thr182) is deep enough to accommodate aromatic residues Tyr178 of cyclin A and Trp95 of cyclin E in the cyclin/CDK2 complex. Therefore, if a small-molecule ligand occupies this cavity, it would disrupt a tight interaction between cyclin E and CDK2 at this location. Moreover, there exist two nearby hydrophobic cavities also shown in Fig. 2a: Cavity 1 formed by Cys177, Phe179, Ser181, Pro271, and Asn272 and used by LAALS peptide and Cavity 2 formed by Phe152, Pro155, Ser181, and Leu124. We thus built our initial pharmacophore model to select small-molecule ligands occupying Cavity 3 and possibly extending to Cavity 1 and Cavity 2 by virtual screening.

For the virtual screening studies, we extracted drug-like compounds from the Enamine stock collection by applying a number of filters and then performed high-throughput docking of these compounds onto the binding pocket of CDK2 using the QXP program (see detailed description of the screening procedure in Materials and Methods). The docking results were processed sequentially (also described in Materials and Methods). First, energetic criteria based on the scoring functions of the QXP program were used to remove outliers. Second, geometric criteria were employed to select compounds with three distinct binding modes (or pharmacophore models) as follows. A putative ligand can interact with the pocket by (1) binding to Cavity 3, only forming hydrophobic interactions and multiple hydrogen bonds, or (2) binding to Cavity 3 while reaching out to the adjacent hydrophobic Cavity 2 with strong π–π and hydrophobic interactions with Phe152 phenyl ring anticipated, and finally (3) stretching from Cavity 3 to the adjacent hydrophobic Cavity 1. Without prior knowledge of the binding mode, we pursued all three in parallel by choosing compounds consistent with each of these three modes independently. This led to the final focused library (also termed the first-generation library) of 148 compounds representing all three binding modes as well as chemical diversity. Detailed information of the library is provided in Supplementary Materials. These compounds were evaluated for their potency in HIV-1-infected ACH2, OM10.1, and U1 cells.

Fig. 2. Virtual screening of libraries and the first set of small-molecule inhibitors against HIV-1 LTR. (a) The surface of CDK2 is shown in orange. The LAALS peptide is shown in balls and sticks. Crystallographic positions of Tyr178 of cyclin A (PDB ID: 2UUE, dark blue) and Trp95 of cyclin E (PDB ID: 1W98, magenta) are shown in sticks. The putative binding sites on CDK2 are located in the three cavities indicated. Small-molecule ligands (also referred as peptide mimetics) are screened for Cavity 3 in order to compete against the interaction of cyclin with CDK2, and they are allowed to further extend to Cavity 1 and Cavity 2 for additional hydrophobic interactions. (b) Peptide mimetics that had scored positive from (a) were tested for their ability to inhibit Tat-activated transcription of an integrated HIV-1 LTR. Tzm-bl cells, carrying an integrated LTR-Luc reporter, were transfected with pcTat (1.0 μg). Twenty-four hours after transfection, the cells were trypsinized and re-seeded in a 96-well plate. Cells were permitted to adhere for 3–4 h before addition of 1 or 10 μM of each of the select peptide mimetics. Luciferase activity was measured 48 h after drug treatment using Bright-Glo Luciferase Reagent (Promega). Data shown represent the average of two replicates and are shown as a fold change of luciferase over the Tat control. (c) HLM-1 cells were transfected (electroporated) with Tat protein and incubated overnight. 5×10^4 cells/1 μg of purified Tat protein was used to screen each mimetic. A total of 39 first-generation mimetics were screened on the HLM-1 cells. Drugs were added at 0.01-, 0.1-, 1-, and 10-μM concentrations. Supernatants were assayed for RT 3 days later. Values are shown as IC_{50} for each drug from HLM-1 treated cells. (d) Toxicity assay using luciferase activity from mimetics-treated cells after 48 h. Samples were measured using Bright-Glo Luciferase Reagent (Promega).

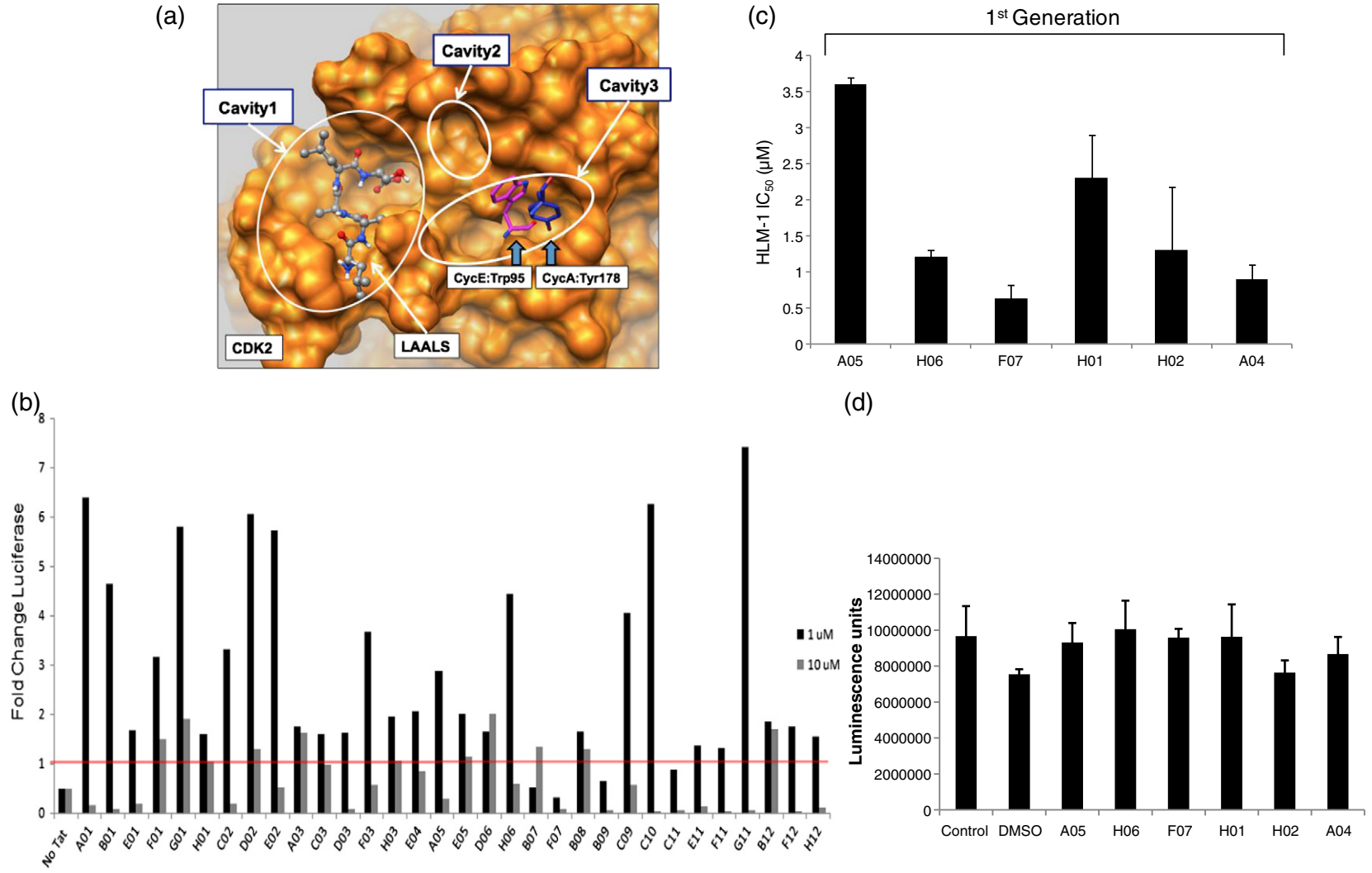

Fig. 2 (*legend on previous page*)

Our initial set of results screening for these 148 compounds showed that some of the compounds were activating the virus and some suppressed virus replication in chronically infected cells (data not shown). We then decided to fine-tune the experiments and use Tzm-bl cells that contain only an HIV-1 LTR Luciferase reporter and can be activated with the addition of exogenous Tat. This would eliminate any off-target effects that may be contributing to non-transcription events during the viral life cycle (present in ACH2, OM10.1, and U1 cells). Results of such an experiment with 32 compounds are shown in Fig. 2b as a fold change in luciferase as compared to Tat transactivation alone, where one compound (F07) was effectively able to decrease transcription more than 10-fold at 1 μM concentrations, and another possible mimetic of interest (B09) decreased transcription by more than 4-fold. An actin Western blot of the two drugs did not show an apparent toxicity in these cells (data not shown). We have also included a representative plot of the screen from Fig. 2b in the presence and absence of Tat to demonstrate that the compounds do not inhibit basal level expression of the HIV-1 LTR and rather are specific for Tat-activated transcription (Supplemental Fig. 1).

To further understand why some of these compounds activated the LTR, we used a series of *in vitro* biochemical assays (dissociation of cyclins from CDKs, titrations with some of the compounds followed by chromatin immunoprecipitation assays, and localization of CDKs in cytoplasm *versus* nucleus) and were unsuccessful in finding out the reason regarding this apparent activation of LTR using compounds other than F07. Upon further examination, we found that many of these compounds in fact activated the CMV promoter that was driving the Tat plasmid used for transfection [using reverse transcription (RT)-PCR and Western blots]. This resulted in the production of higher amounts of Tat protein in cells treated with some of the compounds. For this reason, we went back to re-screening these compounds using HLM-1 cells (HIV-1 wild type/Tat mutant) and performed only transfection with *Escherichia coli* purified Tat protein (1 μg) into these cells. We have previously shown that cells can be electroporated with *E. coli*-made Tat protein and can obtain efficient activated transcription.[10] Using this screen, we found a panel of first-generation inhibitors that suppressed Tat-activated transcription (Fig. 2c) with varying IC_{50} values. Among these compounds, two showed low IC_{50} values (F07 and A04). Using the CellTiter-Glo Assay, we observed no apparent toxicity on these cells using this panel of compounds (Fig. 2d). Therefore, we decided to further pursue the F07 compound in our next set of assays. These results collectively indicate that it may be possible to obtain small-molecule inhibitors that resemble the Tat peptide derivative function to inhibit HIV-1-activated transcription.

From F07 to F07#13 by binding optimization

Hits derived from the *in vitro* screening (F07 and A04 in Fig. 2c) clearly showed a preference toward the second binding mode described above with the ligand occupying Cavity 3 and reaching Phe152 in Cavity 2. Noting that F07 has few rotational bonds but fits very well to Cavity 3, we decided to keep the core region intact and vary only distal groups of the molecule. Using the 5-Ar-3-oxymethyl-Ar-1,2-oxazole pattern, we virtually screened the available compounds from the Enamine database that had the same chemical scaffold and preserved the same pharmacophore interaction mode with CDK2. This resulted in an F07-focused library (termed the second-generation library) of 52 compounds. Details of this library are available in Supplementary Materials.

From this set of 52 compounds, we found 2 compounds with reasonable IC_{50} values (Fig. 3d). One of these compounds, F07#13, with a low IC_{50} (0.12 μM) was further pursued in other assays. Interestingly, F07#13 was found in the virtual screening studies to bind in the same fashion as F07 to Phe152 in Cavity 2 but form a network of more extensive hydrogen bonds with Thr182, Ala277, and Hys119 (Fig. 3a). This more extensive network of hydrogen bonds is consistent with the observed lower IC_{50} for F07#13. Finally, using the assay system in Fig. 2 (HLM-1 cells), we were able to observe more than 90% inhibition when using F07#13 (Fig. 3d). These results collectively indicate that it may be possible to obtain small-molecule drugs that resemble the Tat peptide derivative function to inhibit HIV-1-activated transcription.

Binding specificity of F07 and F07#13 to CDK9

Since the virtual screening that produced F07 and F07#13 was performed for CDK2 and only focused on the interface binding pocket, we also ran global docking simulations of F07 and F07#13 to CDK9 to not only verify their interactions with CDK9 but also study their binding specificity toward different conformations of CDK9. Three different conformations of CDK9 were used: (1) stand-alone CDK9 obtained via homolog modeling from CDK2 (PDB ID: 1E1X) because there is no crystal structure of monomeric CDK9, (2) CDK9/cyclin T1 complex (PDB ID: 3MY1), and (3) CDK9/cyclin T1/Tat complex (PDB ID: 3MI9). The docking protocol is described in Materials and Methods.

The results of our docking simulations of small-molecule ligands, F07 and F07#13, onto CDK9 are summarized in Table 1, which shows the usage of different binding pockets of CDK9, may it be the interface pocket, the well-known ATP pocket, or any other unspecified pockets. According to Table 1, the chance of targeting the interface pocket by both ligands is greatly increased when cyclin T1 is

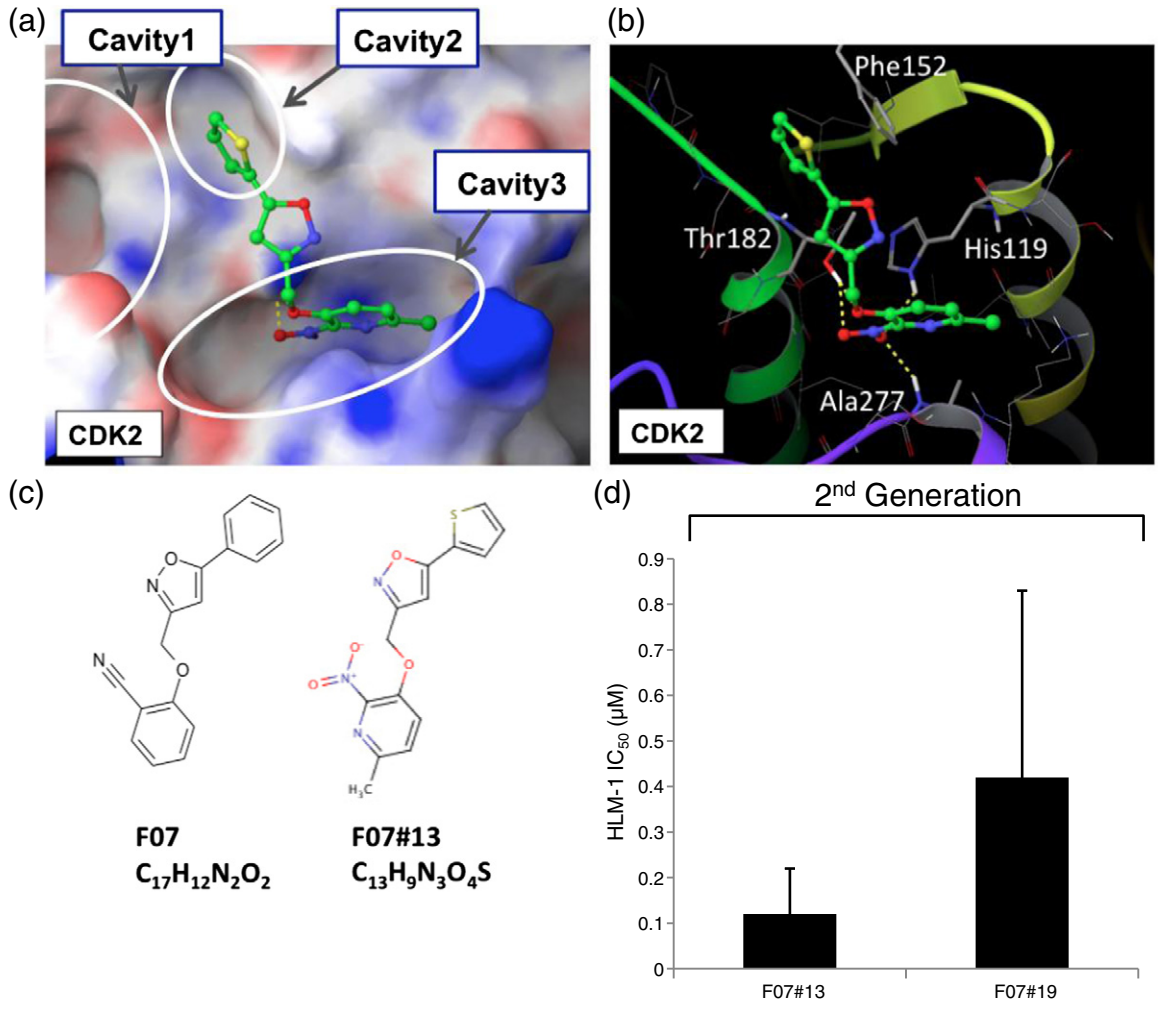

Fig. 3. Binding mode of F07#13 to CDK2. (a) Position of the F07-derived compound F07#13 in the interface binding pocket of CDK2. CDK2 is shown as surface. Cavities in this binding pocket are highlighted. F07#13 straddles Cavity 3 and Cavity 2. (b) Four hydrogen bonds between F07#13 and CDK2 residues are observed and displayed. This shows a network of more extensive hydrogen bonds than that of F07. (c) Structure and chemical composition of F07 and F07#13. (d) Similar to results in Fig. 2, HLM-1 cells were transfected (electroporated) with Tat protein and incubated overnight. A number of second-generation F07 drugs (0.01, 0.1, 1.0, and 10 μM) were screened in a similar manner, two of which with low IC_{50} are shown here.

present, and it even becomes dominant when Tat is also involved. The dominance is mainly due to the sharp increase in the usage of Cavity 2 of the interface pocket. This is particularly interesting since Tat interacts with CDK9 only through Cavity 2. This strongly suggests that both F07 and F07#13 have a clear preference toward targeting the interface pocket disrupting the CDK9/cyclin T1/Tat complex formation when Tat is present, a hypothesis that appears to be supported by the experimental results shown in Fig. 6c. This is significant since it suggests that F07 and F07#13 target the CDK9/cyclin T1 complex predominantly only in HIV-infected cells. The suggested binding modes of F07 and F07#13 also highlighted the differences in their mode of action in CDK2 and CDK9. In the case of the CDK2/cyclin E complex, the two small-molecule inhibitors interfered with Trp95 from cyclin E through a direct competition for Cavity 3. However, in the case of the CDK9/cyclin T1/Tat complex, they affected the complex formation allosterically as neither cyclin T1 nor Tat binds to Cavity 3. Indeed, the crystal structure of the tertiary complex of CDK9/cyclin T1/Tat revealed that all intermolecule interactions occur above the T-loop and Tat interacts with Cavity 2 through the T-loop (Fig. 8).

Compared with the local virtual screening on CDK2, the global docking onto CDK9 also showed some discrepancies. While among the top 10 largest clusters of the docked conformations onto CDK9, there was indeed a binding mode consistent with what was anticipated from the virtual screening on CDK2 (Fig. 3a) given the very close homology

Table 1. Binding specificity of F07 and F07#13 to different conformations of CDK9

Small ligand	Protein complex	PDB ID	Interface binding pocket (%)			ATP pocket (%)	Other pocket (%)
			Cavity 1	Cavity 2	Cavity 3		
F07	CDK9	1E1X	5.1	0.0	9.9	31.8	53.2
	CDK9/cyclin T1	3MY1	32.1	0.0	5.1	50.5	12.3
	CDK9/cyclin T1/Tat	3MI9	39.6	**11.7**	8.6	16.9	23.2
F07#13	CDK9	1E1X	7.9	0.0	9.3	15.7	67.1
	CDK9/cyclin T1	3MY1	31.7	4.9	0.0	48.6	14.8
	CDK9/cyclin T1/Tat	3MI9	35.0	**19.5**	5.3	12.2	28.0

Global docking of F07 and F07#13 onto three different CDK9 structures was performed. The three CDK9 structures studied were (1) stand-alone CDK9 obtained via homolog modeling from CDK2 (PDB ID: 1E1X) because there is no crystal structure of monomeric CDK9, (2) CDK9/cyclin T1 complex (PDB ID: 3MY1), and (3) CDK9/cyclin T1/Tat complex (PDB ID: 3MI9). A total of 600 independent docking runs were conducted against structure (1) and 2400 each against structures (2) and (3). All docked conformations were grouped by cluster analysis, and each and every conformation in the top 10 largest clusters was analyzed to identify which pocket (the interface, the ATP, or other) was used by the ligand (F07 or F07#13) for docking. The table reports the percentage of the pocket usage. For example, in the docking simulation of F07#13 onto the CDK9 structure taken from the CDK9/cyclin T1/Tat complex (PDB ID: 3MI9), 1479 out of 2400 independent runs were clustered into the top 10 largest clusters, and among these 1479 docked conformations, 518 (35%), 288 (19.5%), and 78 (5.3%) went to Cavity 1 entirely, Cavity 2 partly (too small to accommodate the ligand entirely), and Cavity 3 entirely of the interface pocket, respectively (or 35% + 19.5% + 5.3% = 59.8% for the interface pocket); for the remaining conformations, 181 (12.2%) went to the ATP pocket and 414 (28.0%) went to other unspecified pockets. Note that in the presence of the Tat protein, both F07 and F07#13 clearly showed a strong preference in targeting the interface pocket with a sharply increased usage of Cavity 2 of the pocket in particular (marked in boldface).

between the interface pockets of CDK2 and CDK9; there were, however, other binding modes where the ligand either reversed its orientation or targeted different parts of Cavity 3 as shown in Fig. 3a and b. Moreover, the prevailing binding mode observed in the docking simulation was that F07#13 docked entirely into Cavity 1. These discrepancies remain to be resolved experimentally in the future.

Effect of F07#13 on HIV-1 inhibition in primary cells

We next examined the effect of F07#13 on five wild-type and two resistant viruses. Peripheral blood mononuclear cells (PBMCs) were treated with phytohemagglutinin and interleukin (IL)-2 for 2 days and were subsequently infected with five wild-type HIV-1 strains (SF162, BAL, 89.6, JRFL, and ADA). Also, two other resistant strains were tested against the second-generation F07#13 [nevirapine resistant and RTMDRI (resistant to AZT, ddI, nevirapine, and other non-nucleoside reverse transcriptase inhibitors)]. Supernatants of the PBMCs were collected on Days 6 and 9 for RT activity. Results shown are from Day 9 (Fig. 4a). In almost all cases, F07#13 effectively inhibited virus replication in primary cells, and the drug showed no apparent toxicity up to 15-μM concentrations (Fig. 4b). We next asked whether F07 or F07#13 could nonspecifically inhibit CDK9-responsive genes *in vivo*. We utilized a set of cellular and viral genes to test the effect of F07 or F07#13 on their transcription using RT-PCR. Known CDK9-responsive cellular genes included CIITA, MCL-1, cyclin D1, and GAPDH.[11–16] The histone H2B gene served as a negative control for lack of CDK9 requirement for its gene expression.[17] Results in Fig. 4c show that the treatment of cells with F07 or F07#13 (1.2 μM) did not inhibit transcription of genes that were CDK9 responsive, especially in HIV-1-infected cells. We did observe downregulation of CIITA in F07-treated uninfected cells, but there were no changes in genes when treated with F07#13 in either infected or uninfected cells. We explain this as F07 having off-target effects, possibly on the large form of CDK9/cyclin T present in uninfected cells. Future experiments will focus on the third-generation F07#13. This further reinforces the idea that the transcriptional inhibition caused by F07#13 may be specific to the HIV-1 promoter (through Tat modulation of CDK9) and not to cellular genes that utilize the CDK9/cyclin T1 pathway.

Dissociation of CDK9 away from the HIV-1 promoter in the presence of F07#13

We recently showed that CDK9/cyclin T1 exists as at least as four independent p-TEFb complexes in HIV-1-infected cells.[18] One particular complex (Complex IV) was the smallest and was only present in HIV-1-infected Jurkat cells. This complex contained CDK9, cyclin T1, and Hsp70 (or Hsp90) with a molecular mass of ~150 kDa. Log phase growing uninfected and infected pairs (Jurkat/J1.1 and CEM/ACH2) were processed through a sizing column chromatography and low-molecular-weight complexes (III and IV) were Western blotted for the presence of CDK9 and cyclin T1 in order to determine whether the same complex was also detectable in other HIV-1 chronically infected cells. Results in Fig. 5a show that the smaller p-TEFb complex (Complex IV) is mostly present in infected cells, therefore validating our previous results.

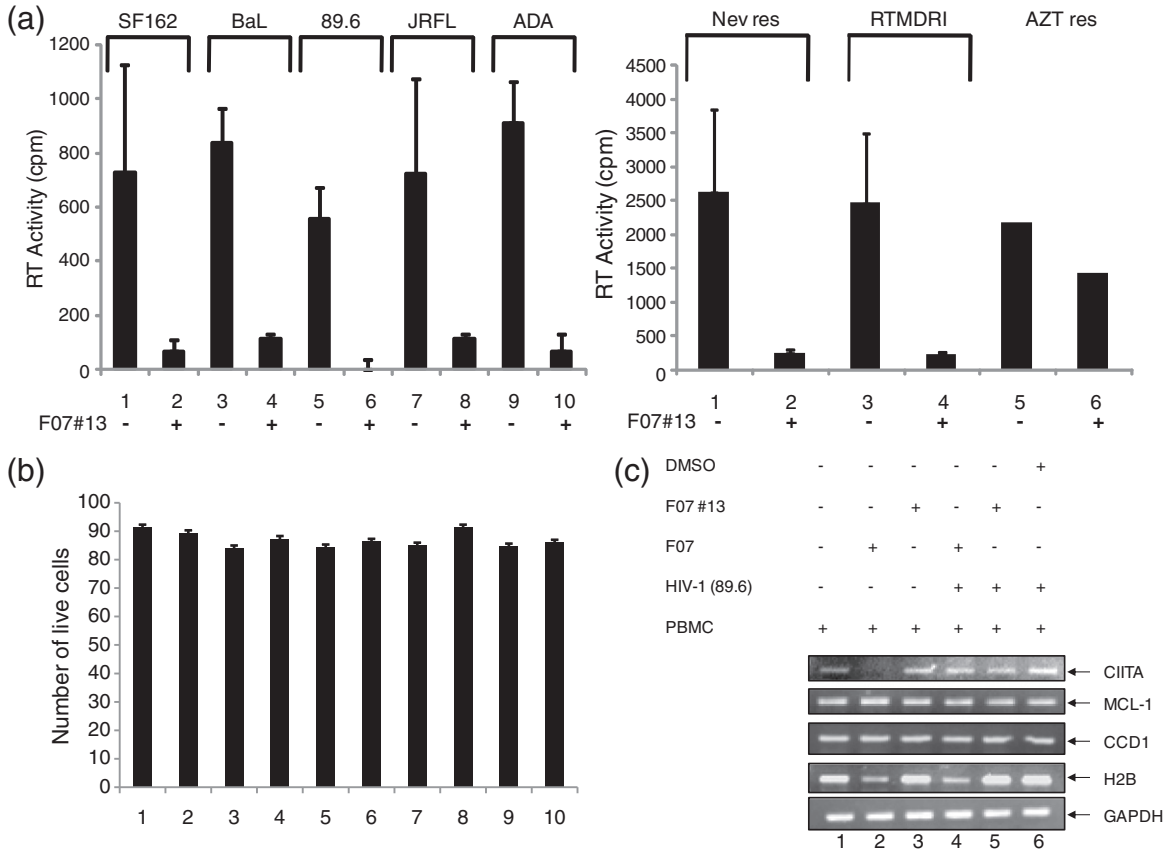

Fig. 4. The effect of F07#13 on HIV-1 replication *in vivo*. (a) Phytohemagglutinin-activated (PHA) and IL-2-activated PBMCs were infected with various strains of virus after 2 days and RT activity was assayed at Day 9. Cells were either untreated or treated with F07#13 (0.12 μM). (b) Activated PBMC cells were treated with increasing concentrations of F07#13 (none, 0.001, 0.01, 0.05, 0.1, 0.5, 1, 5, 10, and 15 μM) for 9 days and cell viability was measured using Trypan blue. Fresh PHA + IL-2 were added every 3 days [same as (a)]. (c) PBMCs were treated with F07 and F07#13 [1.2 μM, 10× of (a)] for 6 days and cells were processed for RT-PCR. Effector CDK9 genes such as CIITA, MCL-1, cyclin D1 (CCD1), H2B, and GAPDH were PCR tested and ran on agarose gels.

Whole cell extracts (lanes 1, 4, 7, and 10) and β-actin serve as positive controls. In order to determine which p-TEFb complex contains the majority of Tat in infected cells, we electroporated CMV-Flag-Tat_{101} (20 μg) into J1.1 cells and subjected the whole cell extracts (~2.5 mg) to elution via size-exclusion chromatography. A panel of every fifth fraction across the elution profile was assayed for the presence of Tat, where ascending fraction numbers correlate to descending molecular weight. Fractions were enriched for Tat using the NT084 (Acid Black 48) nanoparticle (Ceres Nanosciences, Manassas, VA), which we have shown to be capable of specifically binding and trapping HIV-1 Tat from complex and dilute solutions (data not shown). A 30% slurry of nanoparticles was added to each indicated fraction at equal volumes. Samples were incubated with rotation for 30 min at room temperature, spun down, and aspirated, and nanoparticles were resuspended in equal volume of Laemmli buffer for Western blot. Figure 5b demonstrates the distribution of Tat across all four previously described complexes, with raw densitometry counts displayed above each complex. Complex IV contains over 50% of the Tat in infected cells, correlating with the idea that the majority of the Tat in an infected cell binds to the smaller free form of p-TEFb. Interestingly, approximately 30% of the overexpressed Tat also eluted in the high-molecular-weight fractions, indicated as Complex I (p-TEFb complexes that may contain SWI/SNF and other RNA processing components) and 15% in Complex III (p-TEFb complexes that may contain super-elongation components).

We next asked whether F07 or F07#13 was able to dissociate CDK9 away from the HIV-1 transcription complex. We have previously performed similar experiments with our Tat peptide inhibitor.[6,19] We used a transcription strategy (without nucleosomes) where biotinylated LTR DNA was mixed with nuclear extract from which CDK9 has been depleted using an anti-CDK9 antibody (Fig. 6a). We have previously

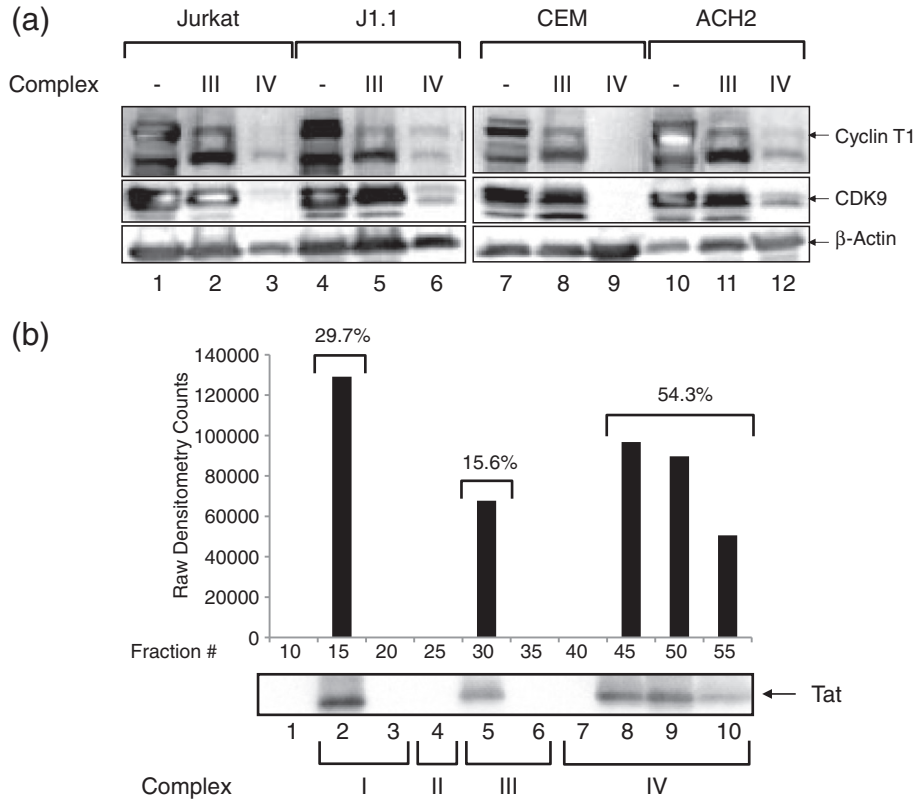

Fig. 5. The incorporation of Tat into unique CDK9/cyclin T-containing complexes. (a) Whole cell extracts from infected (J1.1, ACH2) or uninfected (Jurkat, CEM) cells were loaded onto a sizing column and 0.5-ml fractions were collected at 4 °C. Medium- to small-sized complexes ranging from 500 kDa to 150 kDa were further precipitated (0.25 ml) and ran on a 4–20% SDS/PAGE. Following separation, samples were Western blotted for CDK9, cyclin T1, and actin. Complexes III (~500 kDa) and IV (~150 kDa) show the presence of CDK9, cyclin T1, and β-Actin. (b) HIV-1-infected J1.1 cells were electroporated with 20 μg of CMV-Flag-Tat_{101} and were collected 48 h post-transfection. Cell extracts (~2.5 mg) were eluted off of a size-exclusion chromatography column, and every fifth fraction was enriched for Tat using nanoparticle NT084 and assayed by Western blot. The percentage of total Tat incorporation into each complex is indicated.

utilized this method with an anti-cyclin T antibody; however, the efficiency of the depletion is significantly diminished. We then added back either purified CDK9/cyclin T1 (reminiscent of the free p-TEFb Complex IV) or CDK9/cyclin T1 + Tat complex to the transcription reaction along with F07 or F07#13 (0.1 μM).[5] A silver stain of CDK9/cyclin T1 and CDK9/cyclin T1 + Tat complexes is shown in Fig. 6b. When we performed the add-back experiments in the presence of the two drugs, we found that F07 and F07#13 only dissociated the CDK9 when Tat was present in the complex (Fig. 6c, lanes 5 and 7). The levels of Sp1 loading that bind upstream of the transcription start site did not change in the presence of F07 or F07#13. It is important to note that we have tried to express a Tat/TAR/CDK9/cyclin T1 complex with or without HSP90; however, this purification results in degraded material when using Biotin-TAR RNA as the final bait. We are currently trying to use other approaches including expression *in vitro* (TNT) but have not yet been able to obtain enough material for disassociation experiments. This purified complex would be critical to show that F07 and F07#13 could disrupt this complex through the dissociation of CDK9 in the presence of Tat. These results imply that the CDK9/cyclin T1 complex loaded on the HIV LTR in the presence of Tat may be a distinctly different complex than the normal CDK9/cyclin T1 complex present on the basal HIV or other cellular promoters.

Effect of F07#13 in a humanized mouse model of HIV-1 infection

Finally, we examined if F07#13 could indeed suppress viral replication in the humanized $Rag2^{-/-}\gamma_c^{-/-}$ mice. All six animals utilized were infected with ADA (~100,000 TCID50/ml; administered intraperitoneally) and were divided into three experimental groups, with two animals per group. One group was left untreated and the other groups received either F07 or F07#13 [10 and 100 μg/ml (0.4 and 4 mg/kg), administrated intraperitoneally]. Two weeks after infection, serum samples were

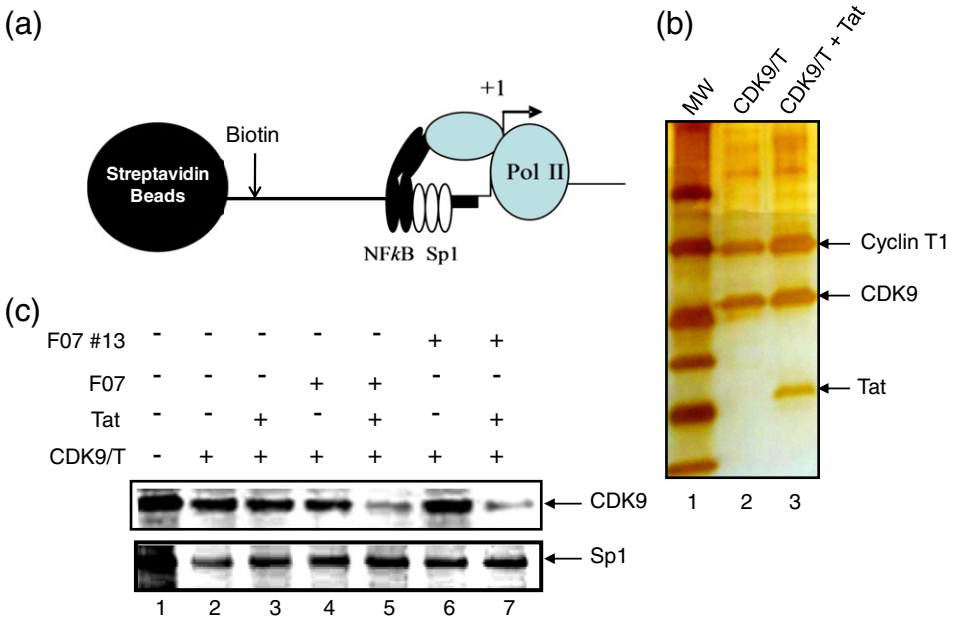

Fig. 6. The effect of F07#13 on HIV-1 transcription *in vitro*. (a) A general diagram of HIV-1 LTR labeled with biotin at the 5′ end used for *in vitro* transcription assays. The sequence contains NF-κB, Sp1, TATA box, and the entire TAR region. *In vitro* transcription was performed with depleted CEM nuclear extract. (b) Silver stain of 1 μg of baculovirus-expressed and purified CDK9/cyclin T1 or CDK9/cyclin T1 + Tat used for transcription reconstitution. (c) Transcription on an immobilized biotinylated HIV-1 LTR template (1 μg/lane). *In vitro* transcription reactions in the presence or absence of CDK9/cyclin T1 or CDK9/cyclin T1 + Tat were incubated for 1 h at 30 °C with only three cold nucleosides (G, C, and U). Transcription reactions were carried with or without F07 or F07#13 (0.1 μM), washed twice, and subsequently stripped with RIPA. Eluted proteins were run on a 4–20% PAGE and Western blotted with anti-CDK9 or anti-Sp1 antibody.

collected from each animal and processed for RT activity as an indication of viremia. Results in Fig. 7 indicate that both F07 and F07#13 are effective in inhibiting HIV-1 *in vivo*. Each bar in the graph is representative of three experimental replicates from the same blood draw. The animals showed no toxicity (up to 3 months after initial treatment of the mimetics; data not shown). Collectively, these results indicate the effectiveness of this class of Tat mimetics and show inhibition of HIV-1 *in vitro* and *in vivo*.

Discussion

In the current study, we attempted to utilize a combination of structure-based analysis of CDK along with previously published Tat peptide derivative. We have been able to model the short Tat peptide inhibitor into pockets of CDK2 and CDK9 (Fig. 1) as well as the peptide and mimetics into pockets of CDK9 (Fig. 8). One particular pocket showed the most stable binding site within Cavity 1 *in silico*. Further analysis of GST-CDK binding

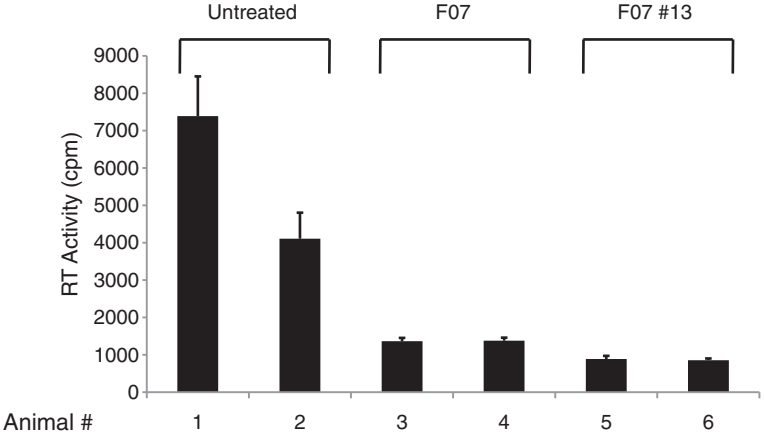

Fig. 7. The effect of F07#13 in a humanized mouse model of HIV-1. Three groups of humanized $Rag2^{-/-}\gamma_c^{-/-}$ mice of two mice each were infected and used for these studies. The treated groups received either F07 or F07#13 [10 and 100 μg/ml (0.4 and 4 mg/kg), administrated intraperitoneally] three times during the 2-week period. Tail blood was collected after 2 weeks and red blood cells were lysed and G-25 cleaned (spun column) prior to RT assay.

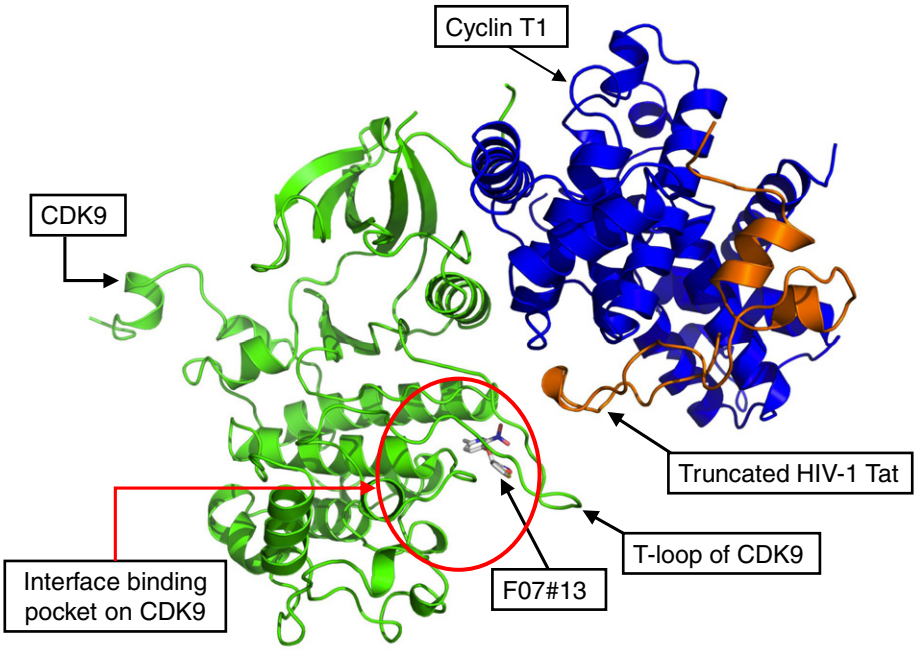

Fig. 8. Complex structure model of CDK9/cyclin T1/Tat. The interface binding pocket on CDK9 is shown where the Tat protein binds. Both the inhibitors (peptide or small molecule) and Tat interact with the T-loop but from opposite sides. For example, the docked F07#13 from our simulation is shown to be located in Cavity 2 of the interface pocket. The interaction with Tat by the inhibitors is indirect and likely through conformational change of the T-loop of CDK9. This mode of interaction may be desirable for not promoting drug resistance.

showed the presence of peaks corresponding to the Tat peptide derivative, LAALS. Using mass spectrometry, we were able to observe a direct binding of the LAALS peptide to CDK9 and not to GST alone.

Furthermore, we were able to find peptide mimetics that bound to similar regions using first *in silico* searches of a chemical library, followed by cell-based assays, and found few inhibitory molecules with reasonable IC_{50} value. It was also surprising to see a few of the compounds that in fact activated the LTR and later turned out to have an activating effect of the drugs on the CMV promoter driving the Tat gene. For that reason, we have relied on delivery of Tat protein into cells to score for LTR activity, which turned out to be a more reliable assay for obtaining data on the true effect of drugs screened in our system. Therefore, using Tat protein transfection, we were able to score for inhibitory activity of a few compounds including the F07 peptide mimetic drug.

We next attempted similar *in silico* analysis and were able to find a second-generation drug resembling F07, where the new target on CDK9 was not only Cavity 1 but also the Cavity 2 region. Four residues at positions D206, S175, N183, and Y185 on CDK9 were critical for this binding *in silico*. More importantly, when examining F07 and F07#13, we observed better binding to the active form of CDK9 in simulations.

When examining the effect of F07#13 on various HIV-1 isolates, we observed a generalized suppression of most viruses. We are currently attempting to use only LTR and Tat sequences from these viruses for transfection in cells and determine whether F07#13 could also inhibit in the LTR/Tat homologous systems. More importantly, this drug does not inhibit well-known CDK9/T-driven cellular genes, which further shows a level of specificity toward HIV-1-associated CDK9/T complex. Other relevant assays also showed the specificity of F07#13 toward dissociation of CDK9, but not SP1, from the HIV-1 promoter. Finally, the drug effectively inhibits viral replication in humanized mouse models of $Rag2^{-/-}\gamma c^{-/-}$ with no toxicity to the animals with concentrations used.

From a mechanistic point of view, we recently discovered that HIV-1-infected cells contain at least four p-TEFb complexes.[18] This is also consistent with a very recent publication from the Rice laboratory where they have discovered more than 12 distinct multi-protein complexes that associate with p-TEFb in HeLa cells.[20] Therefore, the presence of unique CDK9/cyclin T complexes in HIV-1-infected cells is now real and detectable. In our assays, the majority of these complexes have not been fully explored; however, one complex resembles the free/small p-TEFb complex discovered in 2007 using glycerol gradient centrifugation.[21] Using

transfection of an epitope-tag Tat 101 plasmid, followed by chromatography, we recently found that more than half of the Tat is associated with this small complex. This small form of p-TEFb can be inhibited by flavopiridol, ATP analogs such as CR8#13, and Tat peptide mimetics such as F07#13. These inhibitors are effective against this small form of p-TEFb on substrates such as RNA Pol II CTD and histone H1; however, they are not very effective against the other larger forms of p-TEFb at low IC_{50}. Therefore, future experiments comparing these drugs against all four complexes and correlating them with inhibition in latently activated cells as well as humanized mouse model will better differentiate their efficacies *in vivo*.

In conclusion, F07#13 has a distinct inhibitory mechanism different from that of ATP analogs, which may dissociate CDK away from its cyclin partner *in vivo*. This could be due to competition with Tat activity on the CDK molecule.

Materials and Methods

Cell culture and reagents

The uninfected T-cell line, CEM, was obtained from the American Type Culture Collection (Manassas, VA). TZM-bl cells are a HeLa-derived cell line with a stably integrated HIV-1 LTR Luciferase reporter gene. HLM-1 cells are a HeLa-derived cell line, infected with a Tat-negative HIV-1 virus, maintained in the presence of G418. J1.1, ACH2, OM10.1, and U1 cell lines are chronically infected HIV-1 cells of T-cell, promyelocidic, and monocytic origin, respectively. All HIV-1-infected cell lines were obtained from the National Institutes of Health (NIH) AIDS Research and Reference Reagent Program. Suspension cell lines were maintained in RPMI-1640 media containing 10% fetal bovine serum, 1% L-glutamine, and 1% streptomycin/penicillin (Quality Biological, Gaithersburg, MD) at 37 °C in 5% CO_2. Adherent cell lines were maintained in Dulbecco's modified Eagle's medium containing 10% fetal bovine serum, 1% L-glutamine, and 1% streptomycin/penicillin (Quality Biological) at 37 °C in 5% CO_2. The viability of cells was determined by Trypan Blue exclusion assay.

Phytohemagglutinin-activated PBMCs were kept in culture for 2 days prior to each infection. Isolation and treatment of PBMCs were performed by following the guidelines of the Centers for Disease Control and Prevention. Approximately 2.5×10^6 PBMCs were infected with various HIV-1 strains (5 ng of p24 gag antigen). Five wild-type HIV-1 strains—SF162, BAL, 89.6, JRFL, and ADA—were used at 5 ng of p24 virus for each infection. Two other resistant strains—nevirapine resistant [obtained through the AIDS Research and Reference Reagent Program, Division of AIDS, National Institute of Allergy and Infectious Diseases (NIAID), NIH: Nevirapine-Resistant HIV-1 (N119) from Dr. Douglas Richman] and RTMDRI resistant (obtained through the AIDS Research and Reference Reagent Program, Division of AIDS, NIAID, NIH: HIV-1_{RTMDR1} from Dr. Brendan Larder)—were tested against the second-generation drugs. Supernatants were collected on Days 6 and 9 for RT activity. All viral isolates were obtained from the NIH AIDS Research and Reference Reagent Program. After 8 h of infection, cells were washed and fresh medium was added. Drug treatment was performed (only once) immediately after the addition of fresh medium. Samples were collected at various time points and stored at −20 °C for RT assay.

Transfections and RT assays

HIV-1 Tat was expressed in expressing plasmid (pcTat) as previously described.[6,22–25] CMV-Tat (20 μg) or *E. coli* purified Tat protein (1.0 μg) was electroporated into cells as described previously.[10] Viral supernatants (10 μl) were incubated in a 96-well plate with RT reaction mixture containing 1× RT buffer (50 mM Tris–Cl, 1 mM DTT, 5 mM $MgCl_2$, and 20 mM KCl), 0.1% Triton, poly(A) (1 U/ml), pd(T) (1 U/ml), and [^{3}H]TTP. The mixture was incubated overnight at 37 °C, and 10 μl of the reaction mix was spotted on a diethylaminoethyl Filtermat paper, washed four times with 5% Na_2HPO_4 and three times with water, and then dried completely. RT activity was measured in a Betaplate counter (Wallac, Gaithersburg, MD). Cells were also processed for Western blot analysis using anti-actin antibodies.

Western blots

Cell extracts were resolved by SDS-PAGE on a 4–20% Tris–glycine gel (Invitrogen, Carlsbad, CA). Proteins were transferred to Immobilon membranes (Millipore) at 200 mA for 2 h. Membranes were blocked with Dulbecco's phosphate-buffered saline (PBS) + 0.1% Tween-20 + 5% bovine serum albumin. Primary antibody against specified antibodies was incubated with the membrane in PBS + 0.1% Tween-20 overnight at 4 °C. Membranes were washed three times with PBS + 0.1% Tween-20 and incubated with horseradish-peroxidase-conjugated secondary antibody for 1 h. The presence of a secondary antibody was detected by Super Signal West Dura Extended Duration Substrate (Thermo, Rockford, IL).

RT-PCR and primers

For mRNA analysis of CDK9-related genes following drug treatments, total RNA was isolated from cells using Trizol (Invitrogen) according to the manufacturer's protocol. A total of 1 μg of RNA was treated with 0.25 mg/ml DNase I for 60 min, followed by heat inactivation at 65 °C for 15 min. A total of 1 μg of total RNA was used to generate cDNA with the iScript cDNA Synthesis Kit (Bio-Rad, Hercules, CA) using oligo-dT reverse primers.

Peptide synthesis

Peptides used for this study were commercially synthesized (SynBioSci, Livermore, CA). The purity of each peptide was analyzed by HPLC to greater than 98%. Mass spectral analysis was also performed to confirm the identity of each peptide as compared to the theoretical

mass (Applied Biosystems Voyager System 1042, Carlsbad, CA). Peptides were resuspended in ddH_2O to a concentration of 1 mg/ml and stored at −70 °C. Peptides were only thawed once prior to use for biochemical *in vitro* experiments.

GST-CDK binding assay to peptide *in vitro*

GST-CDK9 and GST alone were expressed and purified twice over glutathione Sepharose beads. The elution and re-binding dropped the nonspecific background significantly. Peptides (50 μg) were allowed to bind various purified bead-GST proteins (2 μg) overnight at 4 °C. The next day, they were washed with TNE_{50} + 0.01% NP-40 [50 mM Tris–HCl, 100 mM NaCl, and 0.1 mM ethylenediaminetetraacetic acid (EDTA)] and eluted with 20 μl of elution buffer (TNE_{50} + 0.01% NP-40 + 0.01% SDS). Following centrifugation, eluates were used for further analysis. Eluted peptide samples were zip tipped and then combined with MS washing buffer (50:50 methanol: water + 0.1% trifluoroacetic acid) and loaded onto a Hamilton Gastight 250-μl syringe. Samples were manually injected into an ESI-MS LCQ DecaXP Plus Thermo Finnigan mass spectrometer (Thermo, Hercules, CA) at 10 μl/min and read through an API source. Spectra were normalized to the highest abundant mass peak and were averaged over the course of injection. Data acquisition and peak analysis were performed through the Xcalibur software platforms (Thermo, Hercules, CA). Data are shown zoomed in on relevant *m*/*z* ranges.

Cell viability assay

PBMCs were seeded in 96-well plates at 50,000 cells per well and the inhibitors were added. Cell viability was measured using CellTiter-Glo Cell Luminescence Viability kit (Promega) as per manufacturer's instructions. Briefly, an equal volume of CellTiter-Glo reagent (100 μl) was added to the cell suspension (100 μl). The plate was shaken for approximately 10 min on an orbital shaker at room temperature following which luminescence was detected using the GLOMAX multidetection system (Promega).

Peptide docking

The peptide docking simulations on CDK2 and CDK9 were performed using AutoDock software package version 3.05 (The Scripps Research Institute, La Jolla, CA). For CDK2, the protein receptor, while held rigid, was taken from PDB file 1FIN. For CDK9, the conformation was obtained from PDB file 3BLH. We followed the docking procedure exactly as previously described in detail by Chen *et al.*, including all specific parameters used in the simulated annealing.[8] Global dockings of LAALS onto CDK2 and CDK9 were performed to locate the binding pockets as shown in Fig. 1a and b. In the simulations, several different initial conformations as well as locations of this flexible peptide were chosen at random. For the optimal binding mode (i.e., the lowest-energy docking conformation of highly populated clusters based on a cluster analysis of all resulting docking conformations), the energy contribution toward binding from each residue of CDK2 or CDK9 was computed and ranked using such interactions as van der Waals, hydrogen bond, salvation, and electrostatic terms. The structure of the CDK–peptide complex was visualized in the Chimera program.[26]

Docking of F07 and F07#13 onto CDK9

The docking protocol follows closely the one for peptide docking described above. For each of the two small-molecule ligands F07 and F07#13, three different structures of CDK9 were used for docking simulations: (1) stand-alone CDK9 obtained via homolog modeling from CDK2 (PDB ID: 1E1X) because there is no crystal structure of monomeric CDK9, (2) CDK9/cyclin T1 complex (PDB ID: 3MY1), and (3) CDK9/cyclin T1/Tat complex (PDB ID: 3MI9). After docking simulations for each pair of ligands (F07 or F07#13) and receptors (one of the three CDK9 structures), 600–2400 docking conformations were obtained. A cluster analysis was performed and the threshold was set to 3.0 Å. We then focused on the top 10 largest clusters and located the binding pocket for the lowest docking energy conformation within each cluster by manual inspection. Two pockets are explicitly named, that is, the interface pocket that is further decomposed into three cavities described in the main text and the well-studied ATP pocket.

Virtual screening of small-molecule inhibitors

The interface pocket of CDK2 (PDB IDs: 1W98 and 2UUE), depicted in Fig. 2a, was chosen as the target in virtual screening for small-molecule inhibitors. These inhibitors were also called peptide mimetics because, similar to the peptide inhibitors, they also target the same binding pocket of CDK2. For this purpose, the chemical database Enamine† was selected as our primary source of compounds (~1.6 million currently) because Enamine is one of the largest databases with a guarantee of high-quality supply of purity above 90%. High-throughput docking to the interface pocket was performed for compounds in Enamine that can pass the check of the following rules: (1) Lipinski's Rule of Five, (2) Wever's rules, and (3) 80 or so filters from structural MedChem pattern. At the next step, we converted the compound structure from two dimensions to three dimensions using the LigPrep program and generated isomers (where applicable). The resulting set of the drug-like compounds was subjected for high-throughput docking using the QXP program. One hundred steps of sdock+ routine were used to generate complexes and 10 complexes per ligand were saved.

Processing of docking complexes using three pharmacophore models

The processing of docking complexes was performed sequentially. First, initial energetic filtering was performed with QXP's scoring function to remove outliers. Specifically, we employed QXP scoring function with the following criteria: binding energy $pI > 4.3$ ($pI = -\log_{10} K_i$), hydrogen bonds >1, and distance-dependent ligand–protein contacts $Cntc < -50$. Second, a finer geometric filter, represented by the MultiFilter program developed in-house, was used to identify three putative binding modes.

In the first mode, compounds that bind within Cavity 3 only and form both hydrophobic and multiple hydrogen bonds were selected, whose geometric center must be within 7.5 Å from the amide nitrogen of Ala277. In the second mode, a putative ligand had to bind to Cavity 3 and yet reach the adjacent hydrophobic Cavity 2 formed by Leu124, Phe152, Ser181, and Pro155 residues. Here, two distance filters were applied: 4 Å from the amide nitrogen of Ala277 and 5 Å from the amide nitrogen of Val157. Within this mode, we anticipated strong π–π and hydrophobic interaction with the Phe152 phenyl ring. Finally, we evaluated the binding mode where a ligand stretches from Cavity 3 to the adjacent hydrophobic Cavity 1 formed by Cys177, Phe179, Ser181, Pro271, and Asn272. Hence, putative ligands had to be within at most 4.5 Å away from the Cys177 sulfur atom and at most 4 Å away from the amide nitrogen of Ala277. All compounds that survived from these geometric filters were visually inspected and classified by binding mode and chemotype. Without prior knowledge of the binding mode, we pursued all three in parallel by choosing compounds consistent with each of these three modes independently. This led to the final focused library (also termed the first-generation library) of 148 compounds representing all three binding modes as well as chemical diversity.

Size-exclusion chromatography

Early–mid log phase HIV-1-infected J1-1 and ACH2 cells, uninfected Jurkat and CEM cells, or Flag-Tat_{101} transfected J1.1 cells were pelleted for analysis. Cell pellets were washed twice with PBS without Ca^{2+} and Mg^{2+}, resuspended in lysis buffer [50 mM Tris–HCl (pH 7.5), 120 mM NaCl, 5 mM EDTA, 0.5% NP-40, 50 mM NaF, 0.2 mM Na_3VO_4, 1 mM DTT, and one complete protease cocktail tablet/50 ml], and incubated on ice for 20 min, with gentle vortexing every 5 min. Lysates were then centrifuged at 4 °C at 10,000 rpm for 10 min. Supernatants were transferred to a fresh tube and protein concentrations were determined using the Bradford protein assay (Bio-Rad). Two milligrams of protein from each treatment was equilibrated and degassed in chromatography running buffer [0.2 M Tris–HCl (pH 7.5), 0.5 M NaCl, and 5% glycerol]. The lysates were run on a Superose 6 10/300 size-exclusion chromatography column (GE Healthcare Bio-Sciences, Uppsala, Sweden) using the ÄKTA Purifier system (GE Healthcare Bio-Sciences, Piscataway, NJ, USA). A quarter-inch gap was introduced to the top of the Superose 6 column to better separate low-molecular-weight complexes from fractions eluting off the far right side of the chromatogram. After sample injection (using 1 ml loop), running buffer was set at a flow rate of 0.3 ml/min and 0.5-ml fractions of the flow-through were collected at 4 °C for a total of approximately 60 fractions. Every fifth fraction was acetone precipitated using 4 volumes of ice-cold 100% acetone, incubating for 15 min on ice. Lysates were centrifuged at 4 °C for 10 min at 12,000 rpm, supernatants were removed, and the pellets were allowed to dry for a few minutes at room temperature. The pellets were resuspended in Laemmli buffer and analyzed by immunoblotting for Tat [a cocktail of HIV-1 Tat Monoclonal (4D5.24), HIV-1 Tat Monoclonal (7D5.1), HIV-1 Tat Monoclonal (5A5.3), and HIV-1 Tat (NT3 2D1.1) from Dr. Jonathan Karn, obtained through the AIDS Research and Reference Reagent Program, Division of AIDS, NIAID, NIH], cyclin T1 (Santa Cruz Biotechnology Inc., H-245), CDK9 (Santa Cruz Biotechnology Inc., C-20), and β-actin (Abcam, AB49900). Equal volumes of sample fractions (# 30 and #50) from Jurkat, J1-1, CEM, and ACH2 were loaded on gels prior to Western blots. Additionally, every fifth fraction from J1.1 cells electroporated with Flag-Tat_{101} was screened for the elution of Tat.

Nanoparticle synthesis

The nanoparticle NT084 (Acid Black 48) was generously provided by Ceres Nanosciences. The nanoparticles were synthesized as previously described.[27,28] Briefly, core particles were generated in the following manner: *N*-isopropylacrylamide, *N*′*N*-methylene bisacrylamide, and methyl acrylate were polymerized via precipitation polymerization. The resultant core particles were saponified in lithium hydroxide. Following saponification, the core particles were functionalized with amino dyes via an amidation reaction in dimethylformamide with a dye/methyl acrylate molar ratio of 1:1. After dye incorporation was completed, the dye-functionalized core particles were washed in dimethylformamide and reconstituted in water.

Nanoparticle enrichment of Tat in J1.1 fractions

To prepare size-exclusion chromatography fraction samples for downstream Western blot analysis of FLAG-Tat_{101}, we added a 30% slurry of NT084 (Acid Black 48) to equal volumes of each indicated fraction (15 µl). After rotation for 30 min at 25 °C, samples were centrifuged at 12,000 rpm for 30 s. Supernatants were aspirated, and Laemmli buffer (15 µl) was added to elute materials off of the nanoparticles. Nanoparticles were incubated at −20 °C for 10 min and then vortexed and heated at 95 °C for 5 min. Next, the nanoparticles were centrifuged at 10,000 rpm for 5 min, and the entire volume of Laemmli was loaded onto the gel.

In vitro transcription reaction

In vitro transcription was performed with CEM whole-cell extracts (25 to 50 µg total) on immobilized HIV-1 LTR templates. The DNA fragments were biotinylated, gel purified, and used for *in vitro* transcription. The biotinylated DNA were then incubated at 30 °C for 1 h with paramagnetic beads coupled to streptavidin in a binding buffer containing 10 mM Hepes (pH 7.8), 50 mM KCl, 5 mM DTT, 5 mM PMSF, 5% glycerol, 0.25 mg/ml bovine serum albumin, and 2 mM $MgCl_2$, supplemented with 300 mM KCl. *In vitro* transcription reactions were incubated for 1 h at 30 °C and contained the nucleoside triphosphates ATP, GTP, and CTP at a final concentration of 50 µM and [^{32}P]UTP (20 µCi, 400 Ci/mmol; Amersham, Piscataway, NJ) in buffer D [10 mM Hepes (pH 7.9), 50 mM KCl, 0.5 mM EDTA, 1.5 mM dithiothreitol, 6.25 mM $MgCl_2$, and 8.5% glycerol]. Transcription reactions were terminated by the addition of 20 mM Tris–HCl (pH 7.8), 150 mM NaCl, and 0.2% SDS. For the presence of the RNA molecules, the quenched reactions were extracted with equal volumes of phenol–chloroform

and precipitated with 2.5 volumes of ethanol and 1/10 volume of 3 M sodium acetate (data not shown). Following centrifugation, the RNA pellets were resuspended in 8 μl of formamide denaturation mix containing xylene cyanol and bromophenol blue, heated at 90 °C for 3 min, and separated at 400 V in a 10% polyacrylamide (19:1 acrylamide–bisacrylamide) gel containing 7 M urea (pre-ran at 200 V for 30 min) in 1×Tris–borate–EDTA. The gels were analyzed with the Molecular Dynamics PhosphorImager screen and radioactivity was quantitated with ImageQuant (data not shown).

For the isolation of DNA-bound protein complexes, *in vitro* transcription was performed with CDK9 and cyclin T1 depleted CEM nuclear extract (10 μg of antibody/100 μg of nuclear extract). CDK9 was depleted from nuclear extracts through incubation with an α-CDK9 antibody overnight at 4 °C, followed by the addition of Protein A+G beads, and subsequent centrifugation. Supernatants are then used for *in vitro* transcription reactions. Baculovirus-expressed CDK9/T or CDK9/T+Tat (1 μg) was used to add back to the *in vitro* transcription reaction (purified CDK9/T/Tat was generated as previously described[5]). *In vitro* transcription reactions in the presence of CDK9/T or CDK9/T+Tat were incubated for 1 h at 30 °C with only three cold nucleosides (G, C, and U). Transcription reactions were carried with or without F07 or F07#13 (0.1 μM), washed twice, and subsequently stripped with RIPA. Eluted proteins were run on a 4–20% PAGE and Western blotted with anti-CDK9 or anti-Sp1 antibody.

Mice

A set of male and female $Rag2^{-/-}\gamma c^{-/-}$ [recombinase activating gene knockout, defective in common γ chain (γ_c) receptor for IL-2, IL-7, IL-15] mice was originally donated by Dr. Anton Berns (The Netherlands Cancer Institute). Subsequent experiments utilized similar animals obtained from Dr. Ramesh Akkina (Colorado State University). Both sets of animals are identical with the animals described by Traggiai *et al.*[29] A breeding colony for this and other humanized mouse models has successfully been established at George Mason University (GMU). All procedures and practices associated with the use of $Rag2^{-/-}\gamma c^{-/-}$ mice were approved by the GMU Committee on Human Research and Committee on Animal Research GMU (IACUC #0188). The GMU Committee on Animal Research was charged with carrying out the regulations of the federal government's Animal Welfare Act governing the care and use of animals in research and instruction. The animals were housed in a BSL2 facility consisting of a Techniplast caging system and all changes were completed in a biosafety hood. Bedding, food, and water were all autoclaved. Animals in the vivarium were monitored almost daily and project protocols were reviewed and approved by the University Animal Use Care Committee.

Animals were sub-lethally irradiated, and 24 h later, the mice were given a 100-μl intraperitoneal injection of 100,000 human $CD34^+$ cord blood stem cells. These stem cells were allowed to differentiate for 8 weeks followed by infection with HIV-1. $CD34^+$ cells were either obtained from Cambrex Bio Science Walkersville, Inc. (Gaithersburg, MD) or prepared from embryonic liver cells using the following method. Cells were separated using the CD34 MicroBead Kit (Miltenyi Biotec, Auburn, CA). This kit formerly termed Direct CD34 Progenitor Cell Isolation Kit is a single-step labeling system that allows for a fairly fast and easy isolation of $CD34^+$ cells. By using direct MicroBeads instead of an indirect labeling system, the washing step during the labeling procedure is abolished and resulting cell loss is avoided. The CD34 MicroBead Kit contained FcR blocking reagent and MicroBeads that were conjugated to the monoclonal mouse antihuman CD34 antibody, QBEND/10. The CD34 antigen is a single-transmembrane glycoprotein that is expressed on human hematopoietic progenitor cells and most endothelial cells. Fluorescent control staining of magnetically labeled cells requires a monoclonal CD34 antibody recognizing an epitope other than QBEND/10 (e.g., clone AC136). All cells were washed with PBS prior to implantation. Each animal was given an intraperitoneal injection of virus, virus plus drug, or RPMI media. The treated sets received either F07 or F07#13 [10 and 100 μg/ml (0.4 and 4 mg/kg), administrated intraperitoneally] three times during the 2-week period. Two weeks after infection, the mice were sacrificed and blood was collected through cardiac puncture for further DNA and RNA analysis.

Statistical analysis

All quantifications are based on data obtained from triplicate experiments. *P* values were calculated using Student's *t* test.

Supplementary data to this article can be found online at http://dx.doi.org/10.1016/j.jmb.2012.12.005

Acknowledgements

We would like to thank the members of the Kashanchi laboratory for experiments and assistance with the manuscript. Further support came from grants from the GMU funds to F.K. and NIH grants AI043894, AI078859, and AI074410. Rachel Van Duyne is a predoctoral student in the Microbiology and Immunology Program of the Institute for Biomedical Sciences at the George Washington University. This work is from a dissertation to be presented to the above program in partial fulfillment of the requirements for the Ph.D. degree.

Received 27 July 2012;
Received in revised form 4 December 2012;
Accepted 5 December 2012
Available online 13 December 2012

Keywords:
ATP analog;
CDK9;
cyclin T1;
viral transactivator;
inhibitors

† www.enamine.net

Abbreviations used:
LTR, long terminal repeat; TAR, *trans*-acting-responsive RNA element; GAPDH, glyceraldehyde 3-phosphate dehydrogenase; PDB, Protein Data Bank; PBMC, peripheral blood mononuclear cell; IL, interleukin; NIH, National Institutes of Health; NIAID, National Institute of Allergy and Infectious Diseases; RT, reverse transcription; PBS, phosphate-buffered saline; EDTA, ethylenediaminetetraacetic acid; GMU, George Mason University.

References

1. Wu-Baer, F., Sigman, D. & Gaynor, R. B. (1995). Specific binding of RNA polymerase II to the human immunodeficiency virus trans-activating region RNA is regulated by cellular cofactors and Tat. *Proc. Natl Acad. Sci. USA*, **92**, 7153–7157.
2. Nguyen, V. T., Kiss, T., Michels, A. A. & Bensaude, O. (2001). 7SK small nuclear RNA binds to and inhibits the activity of CDK9/cyclin T complexes. *Nature*, **414**, 322–325.
3. Michels, A. A., Nguyen, V. T., Fraldi, A., Labas, V., Edwards, M., Bonnet, F. *et al.* (2003). MAQ1 and 7SK RNA interact with CDK9/cyclin T complexes in a transcription-dependent manner. *Mol. Cell. Biol.* **23**, 4859–4869.
4. Yang, Z., Zhu, Q., Luo, K. & Zhou, Q. (2001). The 7SK small nuclear RNA inhibits the CDK9/cyclin T1 kinase to control transcription. *Nature*, **414**, 317–322.
5. Tahirov, T. H., Babayeva, N. D., Varzavand, K., Cooper, J. J., Sedore, S. C. & Price, D. H. (2010). Crystal structure of HIV-1 Tat complexed with human P-TEFb. *Nature*, **465**, 747–751.
6. Agbottah, E., Zhang, N., Dadgar, S., Pumfery, A., Wade, J. D., Zeng, C. & Kashanchi, F. (2006). Inhibition of HIV-1 virus replication using small soluble Tat peptides. *Virology*, **345**, 373–389.
7. Deng, L., Wang, D., de la Fuente, C., Wang, L., Li, H., Lee, C. G. *et al.* (2001). Enhancement of the p300 HAT activity by HIV-1 Tat on chromatin DNA. *Virology*, **289**, 312–326.
8. Chen, H., Van Duyne, R., Zhang, N., Kashanchi, F. & Zeng, C. (2009). A novel binding pocket of cyclin-dependent kinase 2. *Proteins*, **74**, 122–132.
9. Baumli, S., Lolli, G., Lowe, E. D., Troiani, S., Rusconi, L., Bullock, A. N. *et al.* (2008). The structure of P-TEFb (CDK9/cyclin T1), its complex with flavopiridol and regulation by phosphorylation. *EMBO J.* **27**, 1907–1918.
10. Kashanchi, F., Duvall, J. F. & Brady, J. N. (1992). Electroporation of viral transactivator proteins into lymphocyte suspension cells. *Nucleic Acids Res.* **20**, 4673–4674.
11. Carlson, B., Lahusen, T., Singh, S., Loaiza-Perez, A., Worland, P. J., Pestell, R. *et al.* (1999). Down-regulation of cyclin D1 by transcriptional repression in MCF-7 human breast carcinoma cells induced by flavopiridol. *Cancer Res.* **59**, 4634–4641.
12. Kanazawa, S., Okamoto, T. & Peterlin, B. M. (2000). Tat competes with CIITA for the binding to P-TEFb and blocks the expression of MHC class II genes in HIV infection. *Immunity*, **12**, 61–70.
13. Barboric, M., Nissen, R. M., Kanazawa, S., Jabrane-Ferrat, N. & Peterlin, B. M. (2001). NF-kappaB binds P-TEFb to stimulate transcriptional elongation by RNA polymerase II. *Mol. Cell*, **8**, 327–337.
14. Lam, L. T., Pickeral, O. K., Peng, A. C., Rosenwald, A., Hurt, E. M., Giltnane, J. M. *et al.* (2001). Genomic-scale measurement of mRNA turnover and the mechanisms of action of the anti-cancer drug flavopiridol.*Genome Biol.* **2**; RESEARCH0041.
15. Eberhardy, S. R. & Farnham, P. J. (2002). Myc recruits P-TEFb to mediate the final step in the transcriptional activation of the cad promoter. *J. Biol. Chem.* **277**, 40156–40162.
16. Chao, S. H., Walker, J. R., Chanda, S. K., Gray, N. S. & Caldwell, J. S. (2003). Identification of homeodomain proteins, PBX1 and PREP1, involved in the transcription of murine leukemia virus. *Mol. Cell. Biol.* **23**, 831–841.
17. Medlin, J., Scurry, A., Taylor, A., Zhang, F., Peterlin, B. M. & Murphy, S. (2005). P-TEFb is not an essential elongation factor for the intronless human U2 snRNA and histone H2b genes. *EMBO J.* **24**, 4154–4165.
18. Narayanan, A., Sampey, G., Van Duyne, R., Guendel, I., Kehn-Hall, K., Roman, J. *et al.* (2012). Use of ATP analogs to inhibit HIV-1 transcription. *Virology*, **432**, 219–231.
19. Van Duyne, R., Cardenas, J., Easley, R., Wu, W., Kehn-Hall, K., Klase, Z. *et al.* (2008). Effect of transcription peptide inhibitors on HIV-1 replication. *Virology*, **376**, 308–322.
20. Ramakrishnan, R., Liu, H., Donahue, H., Malovannaya, A., Qin, J. & Rice, A. P. (2012). Identification of novel CDK9 and Cyclin T1-associated protein complexes (CCAPs) whose siRNA depletion enhances HIV-1 Tat function. *Retrovirology*, **9**, 90.
21. Sedore, S. C., Byers, S. A., Biglione, S., Price, J. P., Maury, W. J. & Price, D. H. (2007). Manipulation of P-TEFb control machinery by HIV: recruitment of P-TEFb from the large form by Tat and binding of HEXIM1 to TAR. *Nucleic Acids Res.* **35**, 4347–4358.
22. Kashanchi, F., Khleif, S. N., Duvall, J. F., Sadaie, M. R., Radonovich, M. F., Cho, M. *et al.* (1996). Interaction of human immunodeficiency virus type 1 Tat with a unique site of TFIID inhibits negative cofactor Dr1 and stabilizes the TFIID–TFIIA complex. *J. Virol.* **70**, 5503–5510.
23. Berro, R., Kehn, K., de la Fuente, C., Pumfery, A., Adair, R., Wade, J. *et al.* (2006). Acetylated Tat regulates human immunodeficiency virus type 1 splicing through its interaction with the splicing regulator p32. *J. Virol.* **80**, 3189–3204.
24. Agbottah, E., de La Fuente, C., Nekhai, S., Barnett, A., Gianella-Borradori, A., Pumfery, A. & Kashanchi, F. (2005). Antiviral activity of CYC202 in HIV-1-infected cells. *J. Biol. Chem.* **280**, 3029–3042.
25. Kashanchi, F., Shibata, R., Ross, E. K., Brady, J. N. & Martin, M. A. (1994). Second-site long terminal repeat (LTR) revertants of replication-defective human immunodeficiency virus: effects of revertant TATA box motifs on virus infectivity, LTR-directed expression, in vitro RNA synthesis, and binding of basal transcription factors TFIID and TFIIA. *J. Virol.* **68**, 3298–3307.
26. Humphrey, W., Dalke, A. & Schulten, K. (1996). VMD: visual molecular dynamics. *J. Mol. Graphics*, **14**, 27–28.

27. Tamburro, D., Fredolini, C., Espina, V., Douglas, T. A., Ranganathan, A., Ilag, L. *et al.* (2011). Multifunctional core-shell nanoparticles: discovery of previously invisible biomarkers. *J. Am. Chem. Soc.* **133**, 19178–19188.
28. Luchini, A., Geho, D. H., Bishop, B., Tran, D., Xia, C., Dufour, R. L. *et al.* (2008). Smart hydrogel particles: biomarker harvesting: one-step affinity purification, size exclusion, and protection against degradation. *Nano Lett.* **8**, 350–361.
29. Traggiai, E., Chicha, L., Mazzucchelli, L., Bronz, L., Piffaretti, J. C., Lanzavecchia, A. & Manz, M. G. (2004). Development of a human adaptive immune system in cord blood cell-transplanted mice. *Science*, **304**, 104–107.